Journal of Trace Elements in Medicine and Biology 51 (2019) 1–8

Contents lists available at ScienceDirect

Journal of Trace Elements in Medicine and Biology

journal homepage: www.elsevier.com/locate/jtemb

Bioinorganic chemistry

Aggregation of the diabetes-related peptide ProIAPP$_{1-48}$ measured by dynamic light scattering

Emma Shardlow[a], Cassandra Rao[b], Roman Sattarov[b], Ling Wu[c], Paul E. Fraser[c], Christopher Exley[a,*]

[a] The Birchall Centre, Lennard-Jones Laboratories, Keele University, Staffordshire, ST5 5BG, UK
[b] The Huxley Building, Life Sciences, Keele University, Staffordshire, ST5 5BG, UK
[c] Tanz Centre for Research in Neurodegenerative Diseases and Department of Medical Biophysics, University of Toronto, Toronto, Ontario, Canada

ARTICLE INFO

Keywords:
IAPP
ProIAPP
Amylin
Amyloid: aggregation
Copper in biology
Aluminium in biology
Dynamic light scattering

ABSTRACT

Islet amyloid polypeptide (IAPP$_{1-37}$) or amylin is implicated in the aetiology of diabetes. It is found as amyloid along with its precursor ProIAPP$_{1-48}$ in the islets of Langerhans in the pancreas. Metals have been implicated in amyloidogenesis of both IAPP and ProIAPP. Herein we have used dynamic light scattering (DLS) to investigate how Al(III) and Cu(II) influence aggregation of ProIAPP$_{1-48}$ under near-physiological conditions and in a biologically-relevant timeframe. ProIAPP$_{1-48}$ formed primarily sub-micron particles within 5 min (e.g. 470 nm at 15μM peptide) that grew to micron-sized particles (1310 nm) within a 30 min timeframe. Equimolar Al(III) had little influence upon particle size at either 5 (656 nm) or 30 min (1250 nm) while Cu(II) tended to increase particle size over the same time period (731–1300 nm). It is suggested that any effects of Al(III) and Cu(II) reflected their well known tendencies to support β-sheet or amorphous aggregates of ProIAPP$_{1-48}$ respectively.

1. Introduction

Amylin or IAPP is a peptide composed of 37 amino acids that was first discovered as a constituent of amyloid deposits in the islets of Langerhans in individuals diagnosed with diabetes [1]. IAPP is highly amyloidogenic and it is this property that implicates it in the degeneration of islet β cells in diabetes [2]. The precursor to IAPP is the 67 amino acid peptide ProIAPP that upon incomplete processing leads to ProIAPP$_{1-48}$ which has also been found in amyloid deposits in diabetes [3]. Recent research implicates aberrant or incomplete processing of ProIAPP in the aetiology of diabetes [4].

While both IAPP and ProIAPP$_{1-48}$ readily form amyloids in vitro their concentrations in vivo are significantly below saturation and a burgeoning body of research is investigating this conundrum [5]. The aggregation of super-saturated concentrations of IAPP is influenced by aluminium [6,7], iron [7], zinc [7,8] and copper [7]. It remains equivocal as to whether Al(III), Fe(III) and Zn(II) promote amyloid (β sheet) formation while it is clear that Cu(II) prevents IAPP from assembling into β sheet structures [7] as recently confirmed [9–13]. ProIAPP$_{1-48}$ forms amyloid less readily than IAPP and while there are few data on its interactions with metals it is also the case that Cu(II) prevents ProIAPP$_{1-48}$ from forming β sheets of amyloid [12,14,15].

It is widely believed that the cytotoxicity's of IAPP and ProIAPP$_{1-48}$ is related to their propensity to form toxic oligomers during the early stages of amyloid formation [5] and it has been suggested that metals and specifically Cu(II) potentiate toxicity through stabilisation of these oligomeric forms [11,16]. We have used dynamic light scattering to investigate in vitro how Al(III) and Cu(II) influence the immediate aggregation of ProIAPP$_{1-48}$ under near physiological conditions.

2. Materials and methods

2.1. Synthesis and purification of peptide

ProIAPP$_{1-48}$ fragments were synthesised using an Applied Biosystems 433 A peptide synthesiser through the application of standard FMOC-based solid phase methodology. Purification of the peptide was performed using RP HPLC on a POROS 20R2 column using water/acetonitrile mixtures buffered with 0.1% TFA. The peptide content of the purified material (77%) was determined by quantitative amino acid analysis and lyophilised aliquots were stored at −80 °C prior to the preparation of peptide stock solutions.

* Corresponding author.
E-mail address: c.exley@keele.ac.uk (C. Exley).

https://doi.org/10.1016/j.jtemb.2018.09.001
Received 4 April 2018; Received in revised form 16 July 2018; Accepted 4 September 2018

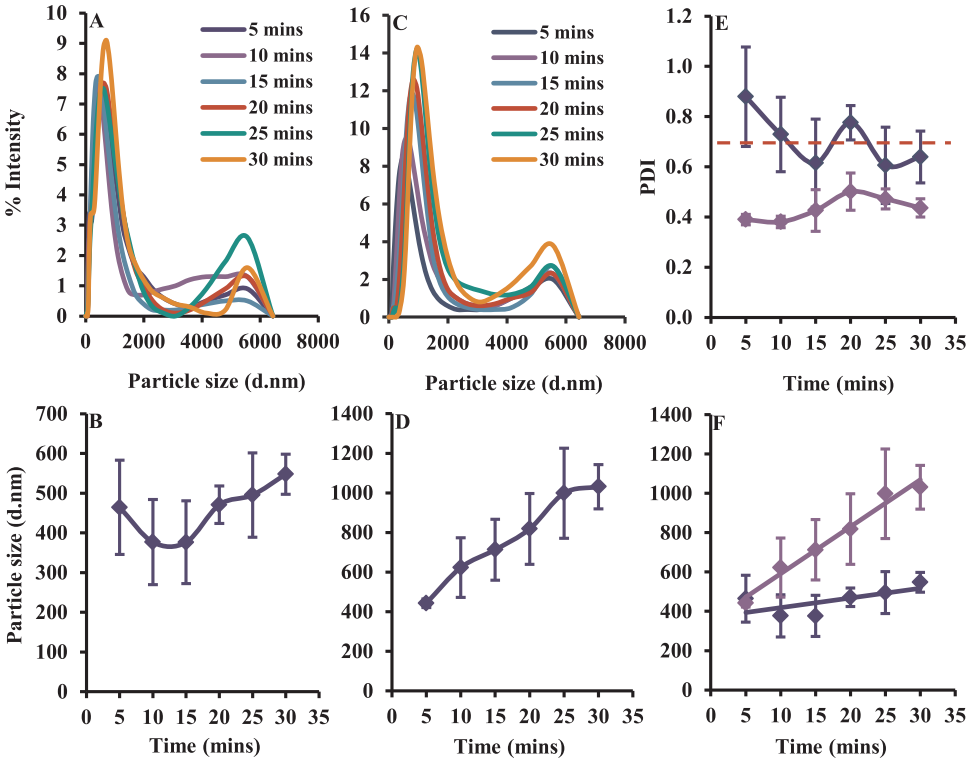

Fig. 1. DLS analyses of ProIAPP$_{1-48}$ in KH buffer over 30 min at 37 °C. Figures A & C represent the raw intensity distributions (d.nm) generated through the measurement of 30 & 60 μM peptide respectively. Figures B & D show the average median particle size (d nm) for 30 & 60 μM peptide respectively. Figures E & F show the PDI values and comparative analysis of the average median particle size data (d.nm) respectively for 30 & 60 μM peptide (blue and purple lines respectively). Error bars represent the ± SD of the measurement where n = 3. The red dotted line on Fig. E illustrates the PDI limit (0.7) over which particle size measurements become unreliable. (For interpretation of the references to colour in this figure legend, the reader is referred to the web version of this article).

2.2. Preparation of peptide stock solutions

Peptide stocks were prepared to a final concentration of 1 mg/mL (*ca* 200 μM) via the addition of ultrapure water (< 0.067 μS/cm) to thawed peptide lyophilisates. This stock was then used to prepare smaller individual volumes of the peptide in order to achieve the final concentrations of peptide included in the following experiments and these aliquots were stored at −20 °C until required.

2.3. Preparation of treatments

To observe the aggregation behaviour of ProIAPP$_{1-48}$ under relevant physiological conditions, thawed peptide aliquots were introduced into two modified Krebs-Henseleit (KH) buffers (pH 7.4 ± 0.05), one containing an absence of citrate and the other supplemented with 1 mM citrate. The final concentrations of peptide included in these treatments were 15, 30 & 60 μM. These represent a range of concentrations from below saturation to concentrations where ProIAPP$_{1-48}$ is known to form amyloid [15]. Treatments containing equimolar concentrations of metal ions (Al^{3+} & Cu^{2+}) were prepared via the addition of certified metal stock solutions (Perkin Elmer, UK) to the KH buffer prior to the introduction of the peptide.

2.4. Particle size analysis

ProIAPP$_{1-48}$ aggregation in the absence and presence of metal ions was monitored by dynamic light scattering (DLS) using a Zetasizer Nano ZS equipped with a 633 nm laser (Malvern Instruments, UK). Samples were prepared in a pre-rinsed quartz low volume cuvette (100 μL) and analysed at 37 °C for 30 min over a range of 0.1–6 μm. Scattered light was detected at an angle of 173° (backscatter) and three measurements consisting of 10 runs each (10 s per run) were conducted per individual sample. These machine replicates were averaged thereafter to obtain the mean distributions generated over a 5-min block and the d50 of these distributions was used in the final analysis. The data shown in the following figures represents the average median particle size of three or six individual sample replicates.

Samples which did not generate enough photonic scattering to generate a reliable distribution (mean count rate < 100 kcps) were deemed to be free of particulates. To ensure the quality of the distributions obtained (see autocorrelation data for all treatments in Supplementary), all accepted measurements had a PDI and multimodal fit error of < 0.7 & < 0.005 respectively, unless otherwise indicated. Measurements of this nature were accepted as of "good" quality in direct accordance with the QC parameters included within the Malvern Zetasizer software.

The size of peptide aggregates was determined using the Stokes-Einstein equation that describes the relationship between hydrodynamic diameter (dh) and velocity of particles within the system undergoing Brownian motion (D) (Eq. (1)).

$$Dh = kT/3\pi\eta D \quad (1)$$

Distributions were generated using a non-negative least squares fit (NNLS) of the correlation function followed by L-curve regularisation.

2.5. Statistical analysis

Statistical analysis of the data was performed using GraphPad Prism software (v.7). The normality of datasets was determined using a Shapiro-Wilk test and those which yielded a p value ≤0.05 were analysed for significance using non-parametric tests. Comparisons over time were performed using a repeated measures ANOVA with a Geisser-Greenhouse correction followed by Tukey post hoc tests or a non-parametric equivalent (Friedman test followed by Dunn post hoc tests). Comparisons between peptide concentration or presence/absence of metals were performed using an ordinary ANOVA followed by Tukey post hoc tests or a non-parametric equivalent (Kruskal-Wallis test followed by Dunn post hoc tests). Comparison of the relative rate of aggregation between samples was performed using linear regression analysis. P values ≤0.05 were considered to be statistically significant.

Table 1
The average median particle size (d.nm ± SD) of ProIAPP$_{1-48}$ (15, 30 & 60 μM) in KH buffer alone or in the presence of equimolar Cu(II) over 30 min at 37 °C (n = 3).

Time (mins)	5	10	15	20	25	30
Concentration of peptide (μM)	**Particle size ± SD (d.nm)**					
Peptide only						
30	464 ± 119	377 ± 107	377 ± 104	471 ± 47	495 ± 106	548 ± 51
60	443 ± 21	622 ± 151	713 ± 154	818 ± 179	998 ± 228	1031 ± 112
Peptide + Cu						
15	251 ± 20	402 ± 84	578 ± 146	631 ± 117	674 ± 111	756 ± 100
30	314 ± 42	534 ± 84	686 ± 93	784 ± 109	928 ± 162	1041 ± 169
60	598 ± 55	998 ± 151	1152 ± 76	1367 ± 47	1397 ± 26	1497 ± 112

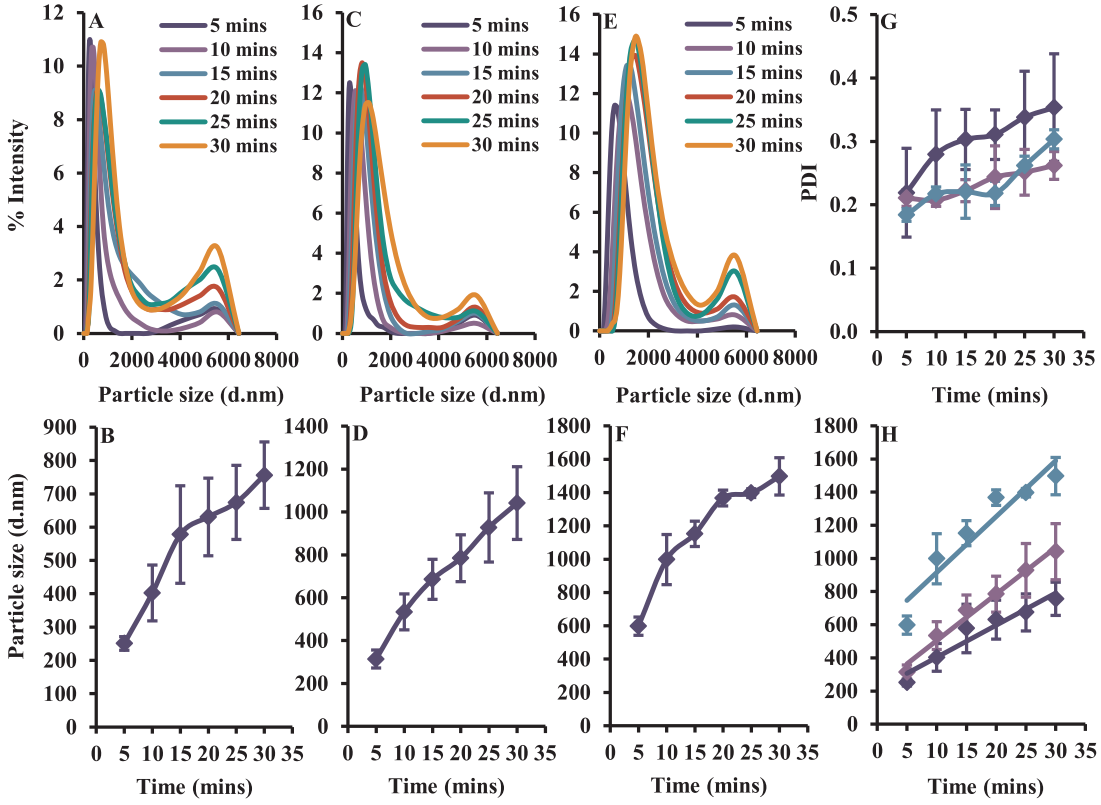

Fig. 2. DLS analyses of ProIAPP$_{1-48}$ + equimolar Cu(II) in KH buffer over 30 min at 37 °C. Figures A, C & E represent the raw intensity distributions (d.nm) generated through the measurement of 15, 30 & 60 μM peptide respectively. Figures B, D & F show the average median particle size (d.nm) for 15, 30 & 60 μM peptide respectively. Figures G & H show the PDI values and comparative analysis of the average median particle size data (d.nm) respectively for 15, 30 & 60 μM peptide (blue, purple & green lines respectively). Error bars represent the ± SD of the measurement where n = 3. (For interpretation of the references to colour in this figure legend, the reader is referred to the web version of this article).

3. Results

3.1. ProIAPP particle size distribution in KH buffer

Particles of ProIAPP could not be measured at a [peptide] of 15 μM at any time point during the 30 min incubation time. Particles of ProIAPP were measured at a [peptide] of 30 and 60 μM at the first time point of 5 min For 30 μM ProIAPP, particles in the sub-micron range were detected at ca 34, 129 and 719 nm and 178 and 786 nm at 5 and 30 min respectively (Fig. 1a). The increase in median particle size from 464 nm at 5 min to 548 nm at 30 min was not statistically significant (Table1; Fig. 1b). The PDI for all samples across each time point ranged from 0.606 to 0.879 casting some doubt upon the reliability of median particle size data (Fig. 1e). For 60 μM ProIAPP, particles in the sub-micron and micron range were detected at ca 52 and 553 nm and 1130 nm at 5 and 30 min respectively (Fig. 1c). The increase in median particle size from 443 nm at 5 min to 1031 nm at 30 min was statistically significant (P = 0.048; Table 1; Fig. 1d). The PDI for all samples across each time point ranged from 0.380 to 0.501 and so median particle size data were considered reliable (Fig. 1e). At the first time point of 5 min the [peptide] had no influence upon particle size whereas at 30 min the particle size was significantly increased at 60μM ProIAPP (P = 0.008; Fig. 1f).

3.2. ProIAPP + Al(III) particle size distribution in KH buffer

While particles were detected at all [peptide] and all time points the commensurate particle distributions were either polydisperse (PDI > 0.700), had a high multimodal fit error or both, factors which rendered median particle size data unreliable (see section 2.4).

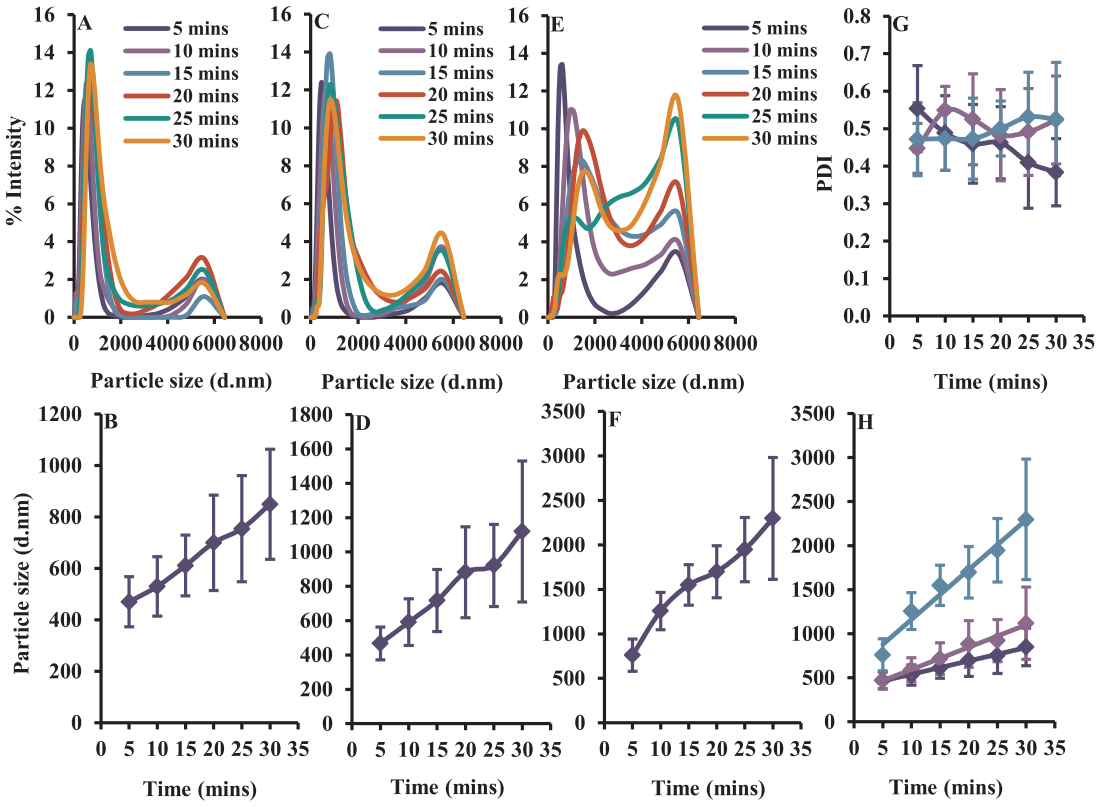

Fig. 3. DLS analyses of ProIAPP$_{1-48}$ in KH buffer + citrate over 30 min at 37 °C. Figures A, C & E represent the raw intensity distributions (d.nm) generated through the measurement of 15, 30 & 60μM peptide respectively. Figures **B, D & F** show the average median particle size (d.nm) for 15, 30 & 60μM peptide (blue, purple & green lines respectively). Figures G & H show the PDI values and comparative analysis of the average median particle size data (d.nm) respectively for 15, 30 & 60 μM peptide (blue, purple & green lines respectively). Error bars represent the ± SD of the measurement where n = 6. (For interpretation of the references to colour in this figure legend, the reader is referred to the web version of this article).

Table 2
The average median particle size (d.nm ± SD) of ProIAPP$_{1-48}$ (15, 30 & 60 μM) in KH + citrate buffer alone or in the presence of equimolar Al(III) or Cu(II) over 30 min at 37 °C (n = 6).

Time (mins)	5	10	15	20	25	30
Concentration of peptide (μM)	**Particle size ± SD (d.nm)**					
Peptide only						
15	470 ± 97	530 ± 116	611 ± 118	699 ± 186	754 ± 206	849 ± 214
30	468 ± 95	591 ± 135	717 ± 181	882 ± 265	922 ± 239	1119 ± 411
60	760 ± 181	1257 ± 209	1549 ± 228	1698 ± 293	1947 ± 360	2298 ± 684
Peptide + Al						
15	686 ± 320	790 ± 53	905 ± 255	1114 ± 576	1111 ± 419	1482 ± 570
30	514 ± 146	782 ± 239	800 ± 255	946 ± 279	1244 ± 488	1087 ± 396
60	717 ± 262	1029 ± 229	1210 ± 234	1594 ± 602	1875 ± 803	1877 ± 863
Peptide + Cu						
15	542 ± 158	774 ± 229	1017 ± 335	1217 ± 439	1201 ± 376	1147 ± 190
30	543 ± 215	835 ± 373	1012 ± 425	1081 ± 332	1321 ± 522	1424 ± 630
60	880 ± 146	1735 ± 295	2110 ± 371	2476 ± 322	2772 ± 319	3037 ± 503

3.3. ProIAPP + Cu(II) particle size distribution in KH buffer

At 15μM ProIAPP, particles were identified at all time points. Particles in the sub-micron range, 304 and 855 nm, were measured at T = 5 and T = 30 min respectively (Fig. 2a). There was a non-significant increase in median particle size from 251 nm after 5 min to 756 nm at 30 min (P = 0.055; Table 1; Fig. 2b). The PDI for all samples across each time point ranged from 0.219 to 0.353 and so median particle size data were considered reliable (Fig. 2g). At 30 μM ProIAPP, particles were identified at all time points. Particles in the sub-micron to micron range, 388 and 1240 nm, were measured at T = 5 and T = 30 min respectively (Fig. 2c). There was a non-significant increase in median particle size from 314 nm after 5 min to 1041 nm at 30 min (P = 0.052; Table 1; Fig. 2d). The PDI for all samples across each time point ranged from 0.207 to 0.262 and so median particle size data were considered reliable (Fig. 2g). At 60μM ProIAPP, particles were identified at all time points. Particles in the sub-micron and micron range, 721 and 1700 nm, were measured at T = 5 and T = 30 min respectively (Fig. 2e). There was a significant increase in median particle size from 598 nm after 5 min to 1497 nm at 30 min (P = 0.021; Table 1; Fig. 2f). The PDI for all samples across each time point ranged from 0.184 to 0.303 and so median particle size data were considered reliable

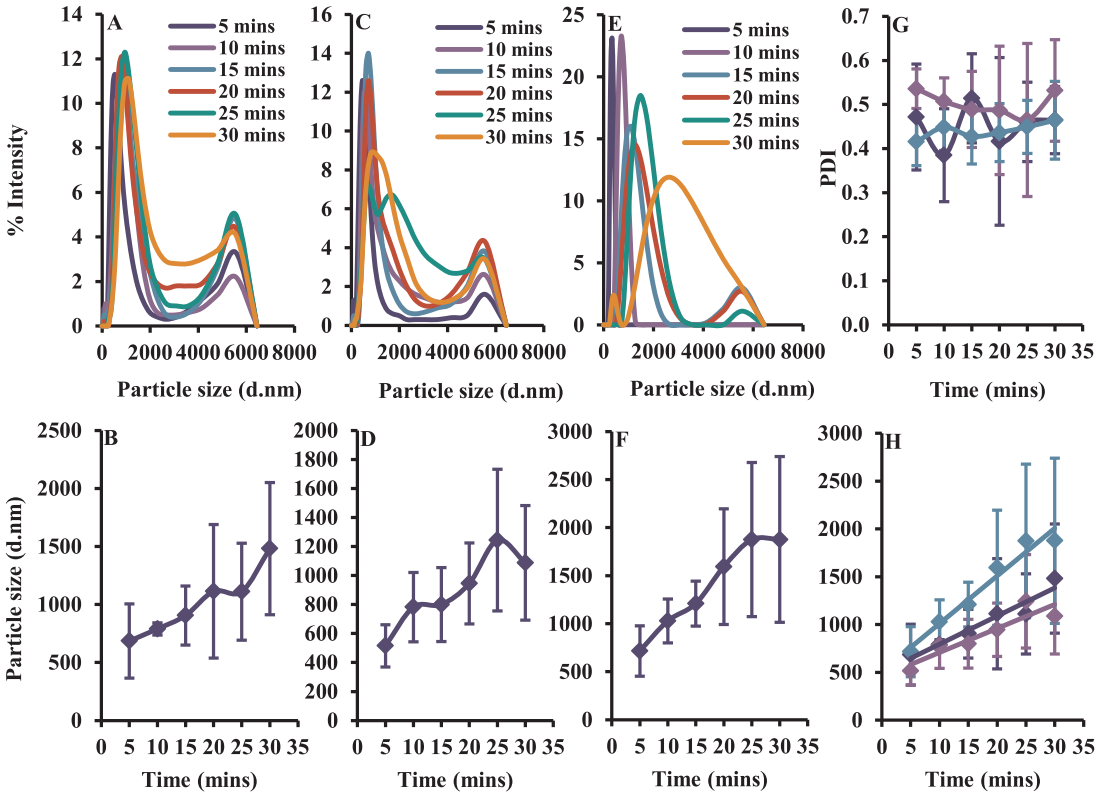

Fig. 4. DLS analyses of ProIAPP$_{1\text{-}48}$ + equimolar Al(III) in KH buffer + citrate over 30 min at 37 °C. Figures A, C & E represent the raw intensity distributions (d.nm) generated through the measurement of 15, 30 & 60 μM peptide respectively. Figures B, D & F show the average median particle size (d.nm) for 15, 30 & 60μM peptide (blue, purple & green lines respectively). Figures G & H show the PDI values and comparative analysis of the average median particle size data (d.nm) respectively for 15, 30 & 60μM peptide (blue, purple & green lines respectively). Error bars represent the ± SD of the measurement where n = 6. (For interpretation of the references to colour in this figure legend, the reader is referred to the web version of this article).

(Fig. 2g). At the first time point of 5 min the median particle size was significantly larger at 60μM than either 15 or 30 μM ProIAPP (P = 0.0001 and 0.0004 respectively; Fig. 2h). At T = 30 min the median particle size was significantly larger at 60 μM than either 15 or 30 μM ProIAPP (P = 0.001 and 0.013 respectively; Fig. 2h). While particle sizes were larger at 30 μM than 15μM at all time points the size differences were not statistically significant (Fig. 2h).

3.4. ProIAPP particle size distribution in KH buffer including citrate

Particles of ProIAPP were measured at [peptide] of 15, 30 and 60 μM at the first time point of 5 min For 15 μM ProIAPP, particles in the sub-micron to micron range were detected at ca 460 nm at 5 min and ca 177 and 1310 nm at 30 min (Fig. 3a). The increase in median particle size from 470 nm at 5 min to 849 nm at 30 min was not statistically significant (P = 0.081) (Table 2; Fig. 3b). The PDI for all samples across each time point ranged from 0.383 to 0.554 and so median particle size data were considered reliable (Fig. 3g). For 30 μM ProIAPP, particles in the sub-micron and micron range were detected at ca 64 and 501 nm and ca 274 and 1080 nm at 5 and 30 min respectively (Fig. 3c). The increase in median particle size from 468 nm at 5 min to 1119 nm at 30 min was not statistically significant (P = 0.082; Table 2; Fig. 3d). The PDI for all samples across each time point ranged from 0.448 to 0.549 and so median particle size data were considered reliable (Fig. 3g). For 60 μM ProIAPP, particles in the sub-micron and micron range were detected at ca 712 nm at 5 min and ca 175, 468 and 1680 nm at 30 min (Fig. 3e). The increase in median particle size from 760 nm at 5 min to 2298 nm at 30 min was statistically significant (P = 0.002; Table 2; Fig. 3f). The PDI for all samples across each time point ranged from 0.448 to 0.549 and so median particle size data were considered reliable (Fig. 3g). At the first time point of 5 min the median particle size for 60μM ProIAPP was significantly larger than for 15 (P = 0.01) and 30μM ProIAPP (P = 0.024). At 30 min the median particle size for 60 μM ProIAPP was significantly larger than for 15 μM ProIAPP (P = 0.004; Fig. 3h).

3.5. ProIAPP + Al(III) particle size distribution in KH buffer including citrate

Particles were measured at [peptide/Al(III)] of 15, 30 and 60 μM at the first time point of 5 min For 15 μM ProIAPP, particles in the sub-micron to micron range were detected at ca 86 and 656 nm at 5 min and ca 1250 nm at 30 min (Fig. 4a). The increase in median particle size from 686 nm at 5 min to 1482 nm at 30 min was statistically significant (P = 0.006) (Table 2; Fig. 4b). The PDI for all samples across each time point ranged from 0.385 to 0.514 and so median particle size data were considered reliable (Fig. 4g). For 30 μM ProIAPP, particles in the sub-micron and micron range were detected at ca 94 and 577 nm and ca 169 and 1160 nm at 5 and 30 min respectively (Fig. 4c). The increase in median particle size from 515 nm at 5 min to 1087 nm at 30 min was statistically significant (P = 0.018; Table 2; Fig. 4d). The PDI for all samples across each time point ranged from 0.465 to 0.536 and so median particle size data were considered reliable (Fig. 4g). For 60 μM ProIAPP, particles in the sub-micron and micron range were detected at ca 337 nm at 5 min and ca 415 and 2800 nm at 30 min (Fig. 4e). The increase in median particle size from 717 nm at 5 min to 1877 nm at 30 min was statistically significant (P = 0.002; Table 2; Fig. 4f). The PDI for all samples across each time point ranged from 0.415 to 0.464 and so median particle size data were considered reliable (Fig. 4g). At the first time point of 5 min the median particle sizes for 15, 30 and 60μM ProIAPP were not statistically different and this trend was also evident at the 30 min time point (Fig. 4h).

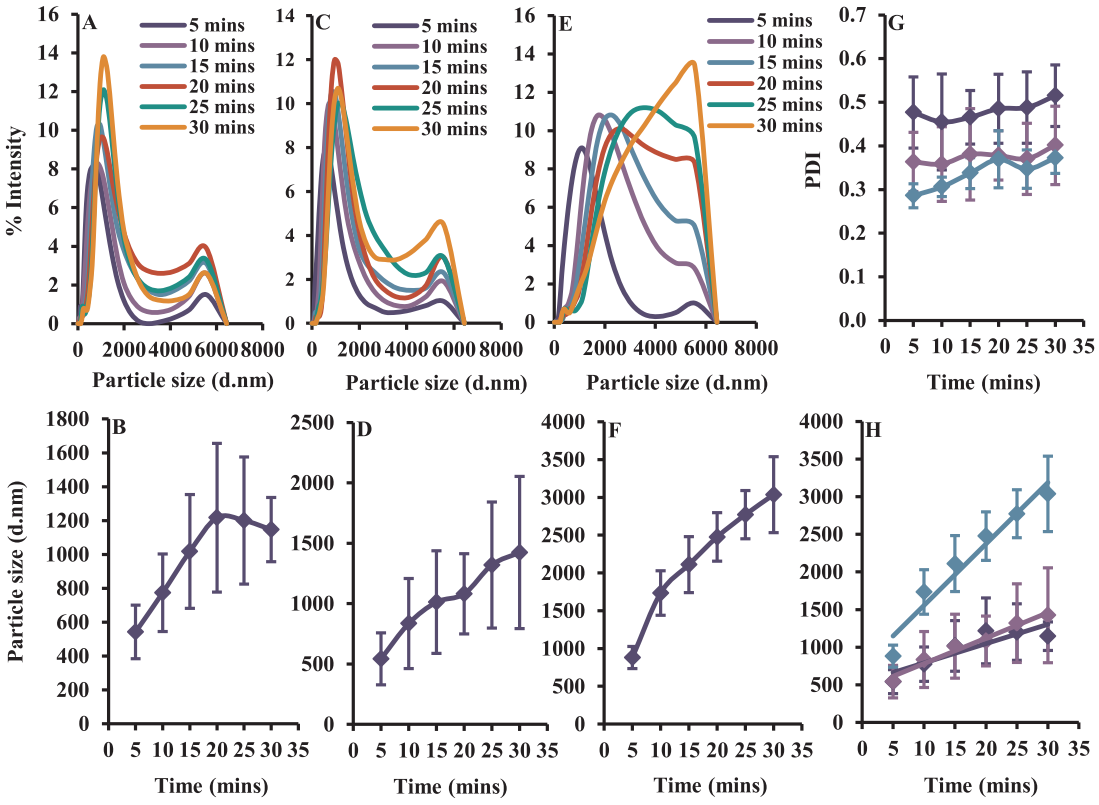

Fig. 5. DLS analyses of ProIAPP$_{1-48}$ + equimolar Cu(II) in KH buffer + citrate over 30 min at 37 °C. Figures A, C & E represent the raw intensity distributions (d.nm) generated through the measurement of 15, 30 & 60μM peptide respectively. Figures B, D & F show the average median particle size (d.nm) for 15, 30 & 60μM peptide (blue, purple & green lines respectively). Figures G & H show the PDI values and comparative analysis of the average median particle size data (d.nm) respectively for 15, 30 & 60μM peptide (blue, purple & green lines respectively). Error bars represent the ± SD of the measurement where n = 6. (For interpretation of the references to colour in this figure legend, the reader is referred to the web version of this article).

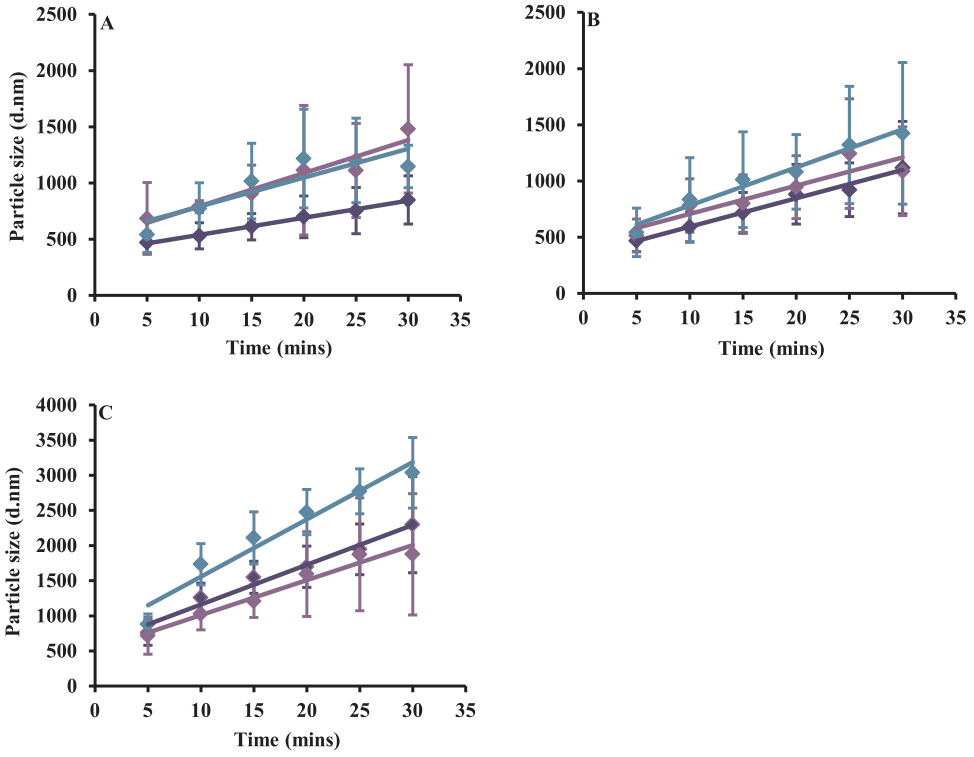

Fig. 6. Comparative analyses of the average median particle size of various concentrations of ProIAPP$_{1-48}$ in KH buffer + citrate in the absence or presence of Al(III) and Cu(II). Figures A, B & C represent 15, 30 & 60 μM peptide respectively alone or in the presence of equimolar Al(III) or Cu(II) (blue, purple & green lines respectively). Error bars represent the ± SD of the measurement where n = 6. (For interpretation of the references to colour in this figure legend, the reader is referred to the web version of this article).

3.6. ProIAPP + Cu(II) particle size distribution in KH buffer including citrate

Particles were measured at [peptide/Cu(II)] of 15, 30 and 60 μM at the first time point of 5 min For 15 μM ProIAPP, particles in the sub-micron to micron range were detected at ca 108 and 731 nm at 5 min and ca 258 and 1300 nm at 30 min (Fig. 5a). The increase in median particle size from 542 nm at 5 min to 1147 nm at 30 min was statistically significant (P = 0.006) (Table 2; Fig. 5b). The PDI for all samples across each time point ranged from 0.455 to 0.515 and so median particle size data were considered reliable (Fig. 5g). For 30 μM ProIAPP, particles in the sub-micron and micron range were detected at ca 677 nm and ca 1280 nm at 5 and 30 min respectively (Fig. 5c). The increase in median particle size from 543 nm at 5 min to 1424 nm at 30 min was statistically significant (P = 0.0005; Table 2; Fig. 5d). The PDI for all samples across each time point ranged from 0.358 to 0.401 and so median particle size data were considered reliable (Fig. 5g). For 60 μM ProIAPP, particles in the sub-micron and micron range were detected at ca 1060 nm at 5 min and ca 435 and 3330 nm at 30 min (Fig. 5e). The increase in median particle size from 880 nm at 5 min to 3037 nm at 30 min was statistically significant (P = 0.0006; Table 2; Fig. 5f). The PDI for all samples across each time point ranged from 0.286 to 0.369 and so median particle size data were considered reliable (Fig. 5g). At the first time point of 5 min the median particle size for 60 μM ProIAPP was significantly larger than for 15 (P = 0.012) and 30 μM ProIAPP (P = 0.012). At 30 min the median particle size for 60 μM ProIAPP was significantly larger than for 15 μM ProIAPP (P = 0.007) and for 30 μM ProIAPP (P = 0.024; Fig. 5h).

4. Discussion

The dilution of 0.2 mM $ProIAPP_{1-48}$ under near-physiological conditions resulted in identifiable particulates of peptide at the first time point of 5 min that increased in size by the final time point of 30 min (Fig. 1). The size of particles increased with [peptide] with no particles being measured at 15μM $ProIAPP_{1-48}$. The majority of particles identified were sub-micron in size though two populations of classical nanoparticles, 34 and 52 nm, were present after 5 min at 30 and 60 μM peptide respectively. Such nanoparticles could not be identified under identical conditions but in the additional presence of equimolar Cu(II) (Fig. 2). Indeed, the presence of Cu(II) increased particle size relative to $ProIAPP_{1-48}$ only preparations (Fig. 6). Unfortunately solubility issues meant that we were unable to obtain reliable data for equimolar Al(III) under these conditions and so we endeavoured to solve this problem by including 1 mM citrate (to reduce the precipitation of aluminium hydroxide) in our physiological medium and repeating all experiments.

The dilution of 0.2 mM $ProIAPP_{1-48}$ under near-physiological conditions in the presence of 1 mM citrate resulted in identifiable particulates of peptide at the first time point of 5 min that increased in size by the final time point of 30 min (Fig. 3). The size of particles increased with [peptide] and while the majority of particles were sub-micron, at 60 μM $ProIAPP_{1-48}$ particles in excess of 2 μm were identified at the 30 min time point. The presence of equimolar Al(III) resulted in reliable data which were very similar to those obtained for $ProIAPP_{1-48}$ only preparations (Fig. 4). While there was evidence that Al(III) increased particle size at 15 μM peptide such differences were not evident at either 30 or 60 μM (Fig. 6). The data for Cu(II) (Fig. 5) supported those obtained in the absence of added citrate in that they showed increases in particle size relative to both $ProIAPP_{1-48}$ only and $ProIAPP_{1-48}$ + Al (III) (Fig. 6) if not statistically significant increases.

We have presented the first data to describe the aggregation of an amyloid-forming peptide under near-physiological conditions within a biologically relevant timeframe. DLS enabled the identification of particles within only 5 min of the initiation of aggregation, something that is not possible by most other methods used in particle sizing. DLS was also effective at a peptide concentration of 15μM, which is close to the solubility of $ProIAPP_{1-48}$ [15]. We have been extremely rigorous in applying quality assurance parameters to ensure that all populations of particles described herein are real and are neither artefacts of control (peptide-free) preparations nor anomalies of the method. There are limitations in that we could not identify populations of particles that were too dilute to produce a robust signal by DLS. However, we have been able to conclude that the particles of $ProIAPP_{1-48}$ identified by DLS were primarily sub-micron, not nanoparticles, growing to several microns in size after 30 min at higher peptide concentrations. In general particle populations identified in the presence of Al(III) were very similar to those of $ProIAPP_{1-48}$ only and such may support the similar particle (fibril) morphologies expected under these conditions. For example, we know that $ProIAPP_{1-48}$ forms amyloid fibrils in a β sheet conformation in both the absence and presence of Al(III) [12,15]. The presence of Cu(II) tended to increase particle sizes, relative to $ProIAPP_{1-48}$ only and $ProIAPP_{1-48}$ + Al(III), across both time points and peptide concentrations and this probably reflected the known amorphous morphologies of Cu(II)-$ProIAPP_{1-48}$ aggregates [12,15]. Herein we could not identify support for either metal acting to stabilise potentially toxic oligomers of $ProIAPP_{1-48}$ (the assumption being that oligomers are classical nanoparticles) as has been suggested for IAPP and other amyloid-forming peptides [5,16,17].

5. Conclusion

An objective of this research was to follow the immediate aggregation of an amyloid-forming peptide as might occur in vivo upon vesicular release of a peptide concentrate into an extracellular milieu. We used a concentration of $ProIAPP_{1-48}$ representative of that secreted into extracellular fluid bathing β-cells in the islets of Langerhans and a buffered system of similar ionic composition to such an environment. DLS successfully captured aggregation events within the first 30 min of vesicular release of peptide and showed that these events were rapid with micron-sized aggregates eventually predominating within the 30-min timeframe. DLS offers a unique opportunity to study such aggregation events in real time and with further optimisation could be applied to a wide range of amyloid-forming peptides. In this way the 'oligomer hypothesis' of the cytotoxicity of amyloid-forming peptides might also be more thoroughly tested.

Conflict of interests

The authors declare no conflict of interests.

Acknowledgements

ES is a CMSRI researchfellow. PEF acknowledges support from the Canadian Institute for Health Research. Dr Caroline Linhart, University of Innsbruck, Austria, is thanked for advice on statistical methods.

Appendix A. Supplementary data

Supplementary material related to this article can be found, in the online version, at doi:https://doi.org/10.1016/j.jtemb.2018.09.001.

References

[1] G.J. Cooper, A.C. Willis, A. Clark, R.C. Turner, R.B. Sim, K.B. Reid, Purification and characterization of a peptide from amyloid-rich pancreases of type 2 diabetic patients, Proc. Natl. Acad. Sci. U. S. A. 84 (1987) 8628–8632.
[2] B. Konarkowska, J.F. Aitken, J. Kistler, S. Zhang, G.J. Cooper, The aggregation potential of human amylin determines its cytotoxicity towards islet beta-cells, FEBS J. 273 (2006) 3614–3624.
[3] P. Westermark, U. Engstrom, G.T. Westermark, K.H. Johnson, J. Permerth, C. Betsholtz, Islet amyloid polypeptide (IAPP) and pro-IAPP immunoreactivity in human islets of Langerhans, Diabetes Res. Clin. Pract. 7 (1989) 219–226.
[4] J.A. Courtade, A.M. Klimek-Abercrombie, Y.-C. Chen, N. Patel, P.Y.T. Lu, C. Speake, P.C. Orban, B. Najafian, G. Meneilly, C.J. Greenbaum, G.L. Warnock,

C. Panagiotopoulos, C.B. Verchere, Measurement of pro-islet amyloid polypeptide (1-48) in diabetes and islet transplants, J. Clin. Endocrinol. Metab. 102 (2017) 2595–2603.
[5] D. Raleigh, X. Zhang, B. Hastoy, A. Clark, The β cell assassin: IAPP cytotoxicity, J. Mol. Endocrinol. 59 (2017) R121–R140.
[6] C. Exley, O. Korchazhkina, Promotion of formation of amyloid fibrils by aluminium adenosine triphosphate (AlATP), J. Inorg. Biochem. 84 (2001) 215–224.
[7] B. Ward, K. Walker, C. Exley, Cu(II) inhibits the formation of amylin amyloid in vitro, J. Inorg. Biochem. 102 (2008) 371–375.
[8] J.R. Brender, K. Hartman, R.P.R. Nanga, N. Popovych, R.D. Bea, S. Vivekanandan, E.G.N. Marsh, A. Ramamoorthy, Role of zinc in human islet amyloid polypeptide aggregation, J. Am. Chem. Soc. 132 (2010) 8973–8983.
[9] L. Ma, X. Li, Y. Wang, W. Zheng, T. Chen, Cu(II) inhibits hIAPP fibrillation and promotes hIAPP-induced beta cell apoptosis through induction of ROS-mediated mitochondrial dysfunction, J. Inorg. Biochem. 140 (2014) 143–152.
[10] H. Li, E. Ha, R.P. Donaldson, A.M. Jeremic, A. Vertes, Rapid assessment of human amylin aggregation and its inhibition by copper (II) ions by laser ablation electrospray ionisation mass spectrometry with ion mobility separation, Anal. Chem. 87 (2015) 9829–9837.
[11] I. Riba, P.E. Barran, G.J.S. Cooper, R.D. Unwin, On the structure of the copper-amylin complex, Int. J. Mass Spectrom. 391 (2015) 47–53.
[12] M. Mold, C. Bunrat, P. Goswami, A. Roberts, C. Roberts, N. Taylor, H. Taylor, L. Wu, P.E. Fraser, C. Exley, Further insight into the role of metals in amyloid formation by $IAPP_{1-37}$ and $ProIAPP_{1-48}$, J. Diabetes Res. Clin. Metab. 4 (2015) 4.
[13] C. Sánchez-López, R. Cortés-Mejía, M.C. Miotto, A. Binolfi, C.O. Fernández, J.M. del Campo, L. Quintanar, Copper coordination features of human islet amyloid polypeptide: the type 2 diabetes peptide, Inorg. Chem. 55 (2016) 10727–10740.
[14] C. Exley, E. House, T. Patel, L. Wu, P.E. Fraser, Human pro-islet amyloid polypeptide (ProIAPP1-48) forms amyloid fibrils and amyloid spherulites in vitro, J. Inorg. Biochem. 104 (2010) 1125–1129.
[15] C. Exley, M. Mold, E. Shardlow, B. Shuker, B. Ikpe, L. Wu, P.E. Fraser, Copper is a potent inhibitor of the propensity for human $ProIAPP_{1-48}$ to form amyloid fibrils in vitro, J. Diabetes Res. Clin. Med. 1 (2012) 3.
[16] S.J.C. Lee, T.S. Choi, J.W. Lee, H.J. Lee, D.-G. Mun, S. Akashi, S.-W. Lee, M.H. Lim, H.I. Kim, Structure and assembly mechanisms of toxic human islet amyloid polypeptide oligomers associated with copper, Chem. Sci. 7 (2016) 5398–5406.
[17] V. Wineman-Fisher, D.N. Bloch, Y. Miller, Challenges in studying the structures of metal-amyloid oligomers related to type 2 diabetes, Parkinson's disease and Alzheimer's disease, Coord. Chem. Rev. (2016) 327–328 20-26.